

One-Dimensional Transient Dynamic Response of Functionally Graded Spherical Multilayered Media

Ibrahim Abu-Alshaikh and Mehmet Emir Koksal

Department of Mathematics, Fatih University,
Istanbul 34500, TURKEY,
Tel.: +90-212-8890810; Fax +90-212-8890832,
E-Mail: aibrahim@fatih.edu.tr

Abstract

In this study, one-dimensional transient dynamic response of functionally graded spherical multilayered media is investigated. The multilayered medium consists of N different layers of functionally graded materials (FGMs), *i.e.*, it is assumed that the stiffness and the density of each layer vary continuously in the radial direction, but isotropic and homogeneous in the other two directions. The inner surface of the layered composite is assumed to be subjected to uniform time-dependent normal stresses; whereas, the outer surface of the composite body is assumed free of surface traction or fixed. Furthermore, the composite body is assumed to be initially at rest and the layers of the multilayered medium are assumed to be perfectly bonded to each other. The method of characteristics is employed to obtain the solutions of this initial-boundary value problem. The numerical results are obtained and displayed in curves denoting the variations of normal stresses with time at different locations. These curves clearly reveal the scattering effects caused by the reflections and refractions of waves at the boundaries and interfaces. The curves also display the effects of geometric dispersions and the effects of non-homogeneity in the wave profiles. Furthermore, they properly predict the sharp variations in the field variables in the neighborhood of the wave fronts. By suitably adjusting the material constants the results for the special case of isotropic, homogenous and linearly elastic multilayered media are obtained and compared with the available solutions in the literature and very good agreement is found. Moreover, solutions for the case of different FGM layers are also obtained.

Key words: Transient dynamic response, Functionally graded materials, Method of characteristics, Spherical layered media.

1 Introduction

Functionally graded materials (FGMs) are ideal candidates of engineering materials for applications involving severe thermal gradients, ranging from thermal structures

in advanced aircraft and aerospace engines to microelectronics. These materials are continuously or discretely changing their thermal and mechanical properties at the macroscopic or continuum scale. The idea of grading the thermomechanical properties of particulate composites was first conceived by a group of material scientists in Japan (see Refs. [1, 2], for example) who coined the term FGMs to describe this generation of composite materials. Several models of FGMs have been considered for the case where a dynamic load is applied to the outer boundaries of a composite body [3]. Largely two models may be used to deal with transient dynamic response in the inhomogeneous FGM bodies; they are the homogeneous layered model and the inhomogeneous continuous model. In the first type, the FGM layer is subdivided into a large number of homogeneous thin layers each of which has its own constant volume fraction [4]. In the second kind, the FGM plate is subdivided into inhomogeneous layers whose material properties vary continuously in the direction perpendicular to the layering [5, 6]. Ohyoshi [5, 6] has developed an analytical method using linearly inhomogeneous layer elements approach to investigate waves through inhomogeneous structures.

Due to the fact that, the material properties of inhomogeneous FGMs are functions of one or more space variable, wave propagation problems related to FGMs are generally difficult to analyze without employing some numerical approaches. Numerical solutions of one-dimensional stress wave propagation in an FGM plate subjected to shear or normal tractions are discussed by Liu *et al.* [7, 8], by Han *et al.* [9] and by Chiu and Erdoğan [10]. In these studies, the material properties are assumed to vary in the thickness direction and the FGM plate is divided into homogeneous layers [7], linearly inhomogeneous elements [8] or quadratic inhomogeneous layer elements [9]. In [10], the material properties of the FGM plate throughout the thickness direction are assumed to be functions with arbitrary powers. Two-dimensional wave propagation in an FGM plate is, recently, discussed applying a composite wave-propagation model in [11] and using finite element method in [12] to simulate elastic wave propagation in continuously non-homogenous materials. However, to the authors' best knowledge, the transient dynamic response of a single or a multilayered spherical FGM body subjected to a uniform pressure wavelet has not been investigated in literature.

In this paper, the method of characteristics is employed to obtain the solutions. This method has been employed effectively in investigating one and two-dimensional transient wave propagation problems in multilayered plane, cylindrical and spherical layered media [13]–[15]. In these references, the multilayered medium consists of N layers of isotropic, homogeneous and linearly elastic or viscoelastic material with one or two relaxation times. A brief review on combining the method of characteristics with Fourier transform to investigate two-dimensional transient wave propagation in viscoelastic layered media can be found in Abu-Alshaikh *et*

al. [16, 17]. It is well known that, for one-dimensional homogeneous case the characteristic manifold consists of straight lines in the $(r - t)$ plane (here, t : time; r : space variable) and the canonical equations holding on them are ordinary differential equations which can be integrated accurately using a numerical method, such as, implicit trapezoidal rule formula [13]–[17]. However, for the inhomogeneous FGM case, the characteristic manifold consists of nonlinear curves in the $(r - t)$ plane and the canonical equations can be integrated approximately along the characteristic lines by employing a small time discretization. This numerical technique is capable of describing the sharp variation of disturbance in the neighborhood of the wave front without showing any sign of instability or noise. Hence, it can be used conveniently for one-dimensional transient wave propagation through FGMs, or it can be combined with a transformation technique to handle two-dimensional transient wave propagation through FGMs.

2 Formulation of the problem

The spherical multilayered medium which is of finite thickness in r -direction consists of N different layers, see Fig. 1. It is referred to a spherical coordinate system (r, θ, ϕ) , in which θ and ϕ are the angles measured from the positive x - and z -axes, respectively. The material properties in each layer are assumed to be vary continuously in the r -direction, but isotropic and homogeneous in θ and ϕ -directions. The inner surface of the layered medium is assumed to be subjected to a uniform time-dependent pressure wavelet. The outer surface is assumed to be either free of surface traction or fixed, or is subject to surface traction similar to that applied at the inner surface, see Fig. 1. Thus, the problem is a one-dimensional wave propagation problem with displacement components u_θ and u_ϕ vanishing identically and the displacement component in the r -direction being a function of r and t , *i. e.*,

$$\begin{aligned} u_r &= u_r(r, t), \\ u_\theta &= u_\phi = 0. \end{aligned} \quad (1)$$

Thus, the stress equation of motion for a typical layer can be written, in the absence of body forces, as

$$\frac{\partial \tau_{rr}}{\partial r} + \frac{2(\tau_{rr} - \tau_{\theta\theta})}{r} = \rho \frac{\partial v_r}{\partial t}, \quad (2)$$

where τ_{rr} and $\tau_{\theta\theta}$ are the normal stress components in r and θ -directions, respectively, ρ is the mass density of the typical layer considered and v_r is the component of the particle velocity in the r -direction, *i. e.*,

$$v_r = \frac{\partial u_r}{\partial t}. \quad (3)$$

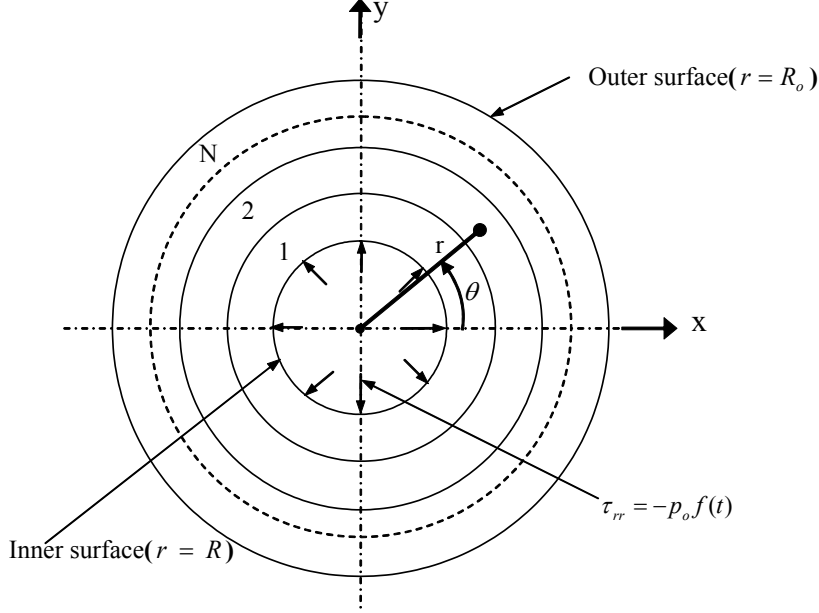


Figure 1: Spherical layered media.

Thus, the nonvanishing stress components can be written as

$$\begin{aligned}\tau_{rr} &= (2\mu + \lambda)\varepsilon_{rr} + 2\lambda\varepsilon_{\theta\theta}, \\ \tau_{\theta\theta} = \tau_{\phi\phi} &= 2(\lambda + \mu)\varepsilon_{\theta\theta} + \lambda\varepsilon_{rr},\end{aligned}\quad (4)$$

where ε_{rr} and $\varepsilon_{\theta\theta}$ ($\varepsilon_{\theta\theta} = \varepsilon_{\phi\phi}$) are the normal strain components for the plane-strain problem considered. These components are related to the nonvanishing displacement component u_r through

$$\varepsilon_{rr} = \frac{\partial u_r}{\partial r}, \quad \varepsilon_{\theta\theta} = \varepsilon_{\phi\phi} = \frac{u_r}{r}.\quad (5)$$

In Eqs. (2) and (4) the stiffness c ($c = 2\mu + \lambda$) and the density ρ of the medium are assumed to be vary continuously in the radial direction, but homogeneous and isotropic in θ and ϕ -directions, that is

$$\begin{aligned}c &= c_0 (a + b r)^m, \\ \rho &= \rho_0 (a + b r)^n,\end{aligned}\quad (6)$$

where a and b are constants representing the gradients of the typical FGM layer. c_0 ($c_0 = 2\mu_0 + \lambda_0$) and ρ_0 are, respectively, the stiffness and mass density at the inner

surface of the typical layer. Similar form of Eq. (6) with $a = 1$ was used by Chiu and Erdoğan [10], in investigating one-dimensional transient wave propagation in an FGM plate subject to a uniform pressure wavelet on one of its outer boundaries. This form of Eq. (6) which is more general than that presented in [10] is selected because it is suitable for a body with a spherical cavity as well as it is suitable for a multilayered medium consists of different FGM layers.

In view of Eq. (6), the constitutive equations, Eqs. (2-5), can be combined in one equivalent equation (wave equation), in terms of the radial displacement (u_r), as

$$c \frac{\partial^2 u_r}{\partial r^2} + \left(\frac{dc}{dr} + \frac{2c}{r} \right) \frac{\partial u_r}{\partial r} + \left(\frac{2}{r} \frac{d\lambda}{dr} - \frac{4\mu}{r^2} \right) u_r = \rho \frac{\partial^2 u_r}{\partial t^2}. \quad (7)$$

In this paper, it is required to solve Eq. (7), satisfying the boundary, initial and interface conditions. The boundary condition at the inner surface ($r = R$) of the multilayered medium is a time-dependent uniform pressure pulse defined as

$$\tau_{rr}(R, t) = -p_o f(t), \quad (8)$$

where p_o is the intensity of the applied load and $f(t)$ is a prescribed function of t . The outer surface $r = R_o$ is assumed to be either free of surface traction, fixed or it can be assumed to be subject to the same load applied at the inner boundary, Eq. (8). Hence, the free or fixed outer boundary conditions can be written, respectively, as

$$\tau_{rr}(R_o, t) = 0 \quad \text{or} \quad u_r(R_o, t) = 0. \quad (9)$$

In the method employed in this study, we note that other alternatives for boundary conditions, such as mixed-mixed boundary conditions on both surfaces, i.e., one component of displacement and the other component of the surface traction can be handled with equal ease on both surfaces. Furthermore, Eq. (8) can be replaced by Eq. (9) at the inner boundary and Eq. (9) can be replaced by Eq. (8) at the outer boundary. The layers of the multilayered medium are assumed to be perfectly bonded to each other; hence, the interface conditions imply that the normal stress (τ_{rr}) and the radial displacement (u_r) are continuous across the interfaces of the layers. The multilayered medium is assumed to be initially at rest; hence, all the field variables are zero at $t \leq 0$. The formulation of the problem is thus now complete.

In view of Eq. (6), the governing field equations, Eqs. (2-5), are to be applied to each layer and the solutions will be required to satisfy the interface conditions at the interfaces, the boundary conditions at inner and outer boundaries, Eqs. (8-9), and quiescent initial conditions.

3 Solution of the problem

The solution is obtained by employing the method of characteristics. This technique involves first writing the constitutive hyperbolic differential equation, Eq. (7), in view of Eqs. (3-6) as a system of first order governing partial differential equations, which can be written in matrix form as

$$\tilde{A}U_{,t} + \tilde{B}U_{,r} + \tilde{F} = \tilde{0} , \quad (10)$$

where

$$\tilde{A} = \tilde{I} , \quad (11)$$

with \tilde{I} being a (6x6) identity matrix. In Eq. (10), \tilde{B} is (6x6) square matrix with the elements all zero except

$$\begin{aligned} b_{16} &= -c, \quad b_{26} = -\lambda, \quad b_{36} = -1, \\ b_{63} &= -\frac{c}{\rho}, \quad b_{64} = -\frac{2\lambda}{\rho}, \quad b_{65} = -\frac{1}{\rho} \frac{dc}{dr}, \end{aligned} \quad (12)$$

\tilde{F} is a six-dimensional column vector with nonzero elements

$$\begin{aligned} f_1 &= -\frac{2\lambda v_r}{r}, \quad f_2 = -\frac{2(\lambda+\mu)v_r}{r}, \quad f_4 = -\frac{v_r}{r}, \\ f_5 &= -v_r, \quad f_6 = -\frac{2(\tau_{rr}-\tau_{\theta\theta})}{r\rho} - \frac{2u_r}{\rho r} \frac{dc}{dr}, \end{aligned} \quad (13)$$

and \tilde{U} is a six-dimensional column vector containing the unknown field variables:

$$\tilde{U} = (\tau_{rr}, \tau_{\theta\theta}, \varepsilon_{rr}, \varepsilon_{\theta\theta}, u_r, v_r)^T , \quad (14)$$

where T designates the transpose. In Eq. (10), comma denotes partial differentiation:

$$\tilde{U}_{,t} = \frac{\partial \tilde{U}}{\partial t}, \quad \tilde{U}_{,r} = \frac{\partial \tilde{U}}{\partial r}, \quad (15)$$

The second step of the solution procedure involves the determination of the solutions of Eq. (10) for each layer satisfying the conditions at the boundaries, Eqs. (8-9), the interface and the zero initial conditions. The system of governing equations, Eq. (10), is hyperbolic, and the solution is constructed by converting it into a system of ordinary differential equations each of which is valid along a different family of characteristic lines. These equations, called the canonical equations, are suitable for numerical analysis, because the use of the canonical form makes it possible to obtain the solution by a step-by-step integration procedure. The convergence and numerical stability of the method are well-established, see Courant and Hilbert [18] and Whitham [19].

The characteristic lines, along which the canonical equations are valid, are governed by the characteristic equation

$$\det(\underset{\sim}{B} - V\underset{\sim}{A}) = 0, \quad (16)$$

where $V = \frac{dr}{dt}$. Eq. (16) yields the eigenvalues V_i ($i = \overline{1,6}$), which are

$$V_1 = c_p, \quad V_2 = -c_p, \quad V_i = 0 \quad (i = \overline{3,6}), \quad (17)$$

where

$$c_p = \sqrt{\frac{c}{\rho}} = \sqrt{\frac{\lambda + 2\mu}{\rho}} = \sqrt{\frac{(2\mu_0 + \lambda_0)(a + br)^m}{\rho_0(a + br)^n}}. \quad (18)$$

The characteristic manifold is thus composed of the families of the curves $\frac{dr}{dt} = V_i$ ($i = \overline{1,6}$). $\frac{dr}{dt} = V_1 = c_p$ and $\frac{dr}{dt} = V_2 = -c_p$ describe two characteristic families of curves with slopes (c_p) and ($-c_p$), respectively, on the $r - t$ plane. $\frac{dr}{dt} = V_i = 0$, ($i = \overline{3,6}$) define straight lines parallel to the t -axis, see Fig. 2.

The canonical equations are determined from

$$\underset{\sim}{\ell}_i^T \underset{\sim}{A} \frac{d\underset{\sim}{U}}{dt} + \underset{\sim}{\ell}_i^T \underset{\sim}{F} = 0, \quad (19)$$

which holds along $\frac{dr}{dt} = V_i$ ($i = \overline{1,6}$). In Eq. (19), $\frac{d}{dt}$ denotes the total time derivative along a characteristic line and $\underset{\sim}{\ell}_i$ is the left-hand eigenvector satisfying the equation

$$\underset{\sim}{B}^T \underset{\sim}{\ell}_i = V_i \underset{\sim}{A}^T \underset{\sim}{\ell}_i. \quad (20)$$

In view of Eqs. (11-12) and (17-18), the linearly independent left-hand set of eigenvectors can be determined from Eq. (20). When these left-hand eigenvectors together with $\underset{\sim}{A}$ and $\underset{\sim}{F}$ defined in Eqs. (11) and (13) are substituted into Eq. (19), the canonical equations can be obtained explicitly as

$$K_{ij} \frac{dU_j}{dt} = H_{ij} U_j \quad (i, j = \overline{1,6}), \quad (21)$$

where the elements of U_j are given in Eq. (14), and the nonzero elements of K_{ij} and H_{ij} , are

$$\begin{aligned} k_{13} &= -c_p, \quad k_{14} = -\frac{2\lambda}{\rho c_p}, \quad k_{15} = -\frac{1}{\rho c_p} \frac{dc}{dr}, \\ k_{23} &= c_p, \quad k_{24} = \frac{2\lambda}{\rho c_p}, \quad k_{25} = \frac{1}{\rho c_p} \frac{dc}{dr}, \quad k_{33} = -\lambda, \\ k_{32} &= k_{16} = k_{26} = k_{41} = k_{65} = k_{54} = 1, \quad k_{43} = -c, \\ h_{11} &= \frac{2}{r\rho}, \quad h_{12} = -\frac{2}{r\rho}, \quad h_{15} = \frac{2}{r\rho} \frac{d\lambda}{dr}, \quad h_{16} = -\frac{2\lambda}{r\rho c_p} - \frac{1}{\rho c_p} \frac{dc}{dr}, \\ h_{21} &= \frac{2}{r\rho}, \quad h_{22} = -\frac{2}{r\rho}, \quad h_{25} = \frac{2}{r\rho} \frac{d\lambda}{dr}, \quad h_{26} = \frac{2\lambda}{r\rho c_p} + \frac{1}{\rho c_p} \frac{dc}{dr}, \\ h_{36} &= \frac{2(\lambda + \mu)}{r}, \quad h_{46} = \frac{2\lambda}{r}, \quad h_{56} = \frac{1}{r}, \quad h_{66} = 1. \end{aligned} \quad (22)$$

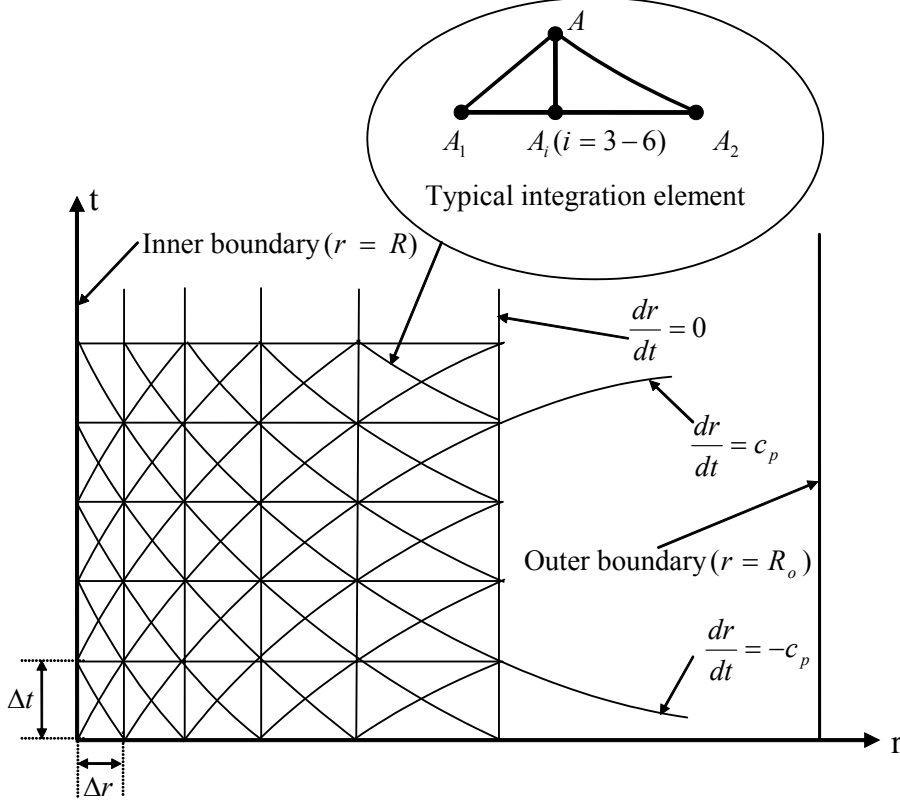


Figure 2: Network of characteristic lines on the $(r - t)$ plane.

The canonical equations are then integrated along the characteristic lines as

$$\int_{A_i}^A K_{ij} \frac{dU_j}{dt} dt - \int_{A_i}^A H_{ij} U_j dt = \underline{0}, \quad (23)$$

where A and A_i are points on the characteristic lines defined, respectively, at current and previous time steps as shown in the typical integration element inside Fig. 2. Taking into consideration that the coefficients K_{ij} and H_{ij} are functions of r only,

the above integration can be performed easily by using the trapezoidal rule as [20]

$$K_{ij}U_j(A) - K_{\underline{i}j}U_j(A_{\underline{i}}) - \left(\frac{\Delta t}{2}\right) \{H_{ij}(A)U_j(A) + H_{\underline{i}j}(A_{\underline{i}})U_j(A_{\underline{i}})\} = \underline{0}. \quad (24)$$

Alternately, this equation can be rewritten as

$$W_{ij}U_j(A) = M_{\underline{i}j}U_j(A_{\underline{i}}) \quad (i, j = \overline{1, 6}), \quad (25)$$

where

$$W_{ij} = K_{ij} - \left(\frac{\Delta t}{2}\right) H_{ij}(A), \quad M_{\underline{i}j} = K_{\underline{i}j} + \left(\frac{\Delta t}{2}\right) H_{\underline{i}j}(A_{\underline{i}}). \quad (26)$$

The elements of K_{ij} and H_{ij} are given in Eqs. (22). In Eqs. (24-26) there is no summation over the underlined index (\underline{i}), therefore, Eq. (25) represents six equations defined by $i = \overline{1, 6}$ and for each value of the index i , there is a summation over j which takes the values $j = \overline{1, 6}$. Thus, when the values of U_j are known at the points A_i ($i = \overline{1, 6}$), the unknown vector $U_j(A)$ can be determined from Eqs. (25). In other words, using the triangular mesh shown inside Fig. 2, the field variables at a specific point along any line parallel to the r -axis in the solution region can be found in terms of the known field variables defined on the previous line. To compute the components of the unknown vector U_j ($j = \overline{1, 6}$) presented in Eqs. (25) at every intersection point between the characteristic lines on the $r - t$ plane, we refer to the network of the characteristic lines, Fig. 2. We start our solution on the network from the r -axis, where the values of all field variables are zero due to the zero initial conditions, and advance into the solution region by computing U_j at the intersection points of the network between the inner and the outer boundary along the lines $t = \Delta t, t = 2\Delta t, t = 3\Delta t, \dots, t = J_{\max}\Delta t, \dots$ etc. To explain this numerical procedure we refer to four different locations of the typical integration element. First, if the typical integration element is located at the inner boundary then the first equation of Eqs. (25), which is valid along the line $A - A_1$ is replaced by the boundary condition applied at the inner boundary. Second, if the integration element is an interior element, then the procedure involves the determination of the values of the unknown vector at a point A in terms of their values at A_1, A_2 and A_i ($i = \overline{3, 6}$) using Eqs. (25). Third, if a point A of the integration element is located at an interface between two different layers then the first two equations are replaced by the interface continuity conditions, whereas, in this case the number of field variables becomes double at that point. Finally, the second equation of Eqs. (25) is replaced by the boundary condition applied at the outer boundary if the typical integration element lies at that boundary. This procedure is repeated as we proceed along the t -axis, for example along the line $t = 2\Delta t$, instead of using the initial conditions along the line $t = 0$, we use the field variables which are

computed in the previous step along the line $t = \Delta t$. This process is repeated until getting results for a sufficient value of t , for example $t = J_{\max}\Delta t$, where J_{\max} is the maximum number of intervals considered in the t -direction.

4 Numerical results and discussion

The first example will be given to verify the validity of the numerical technique employed in this study. The numerical results are obtained for a composite body consisting of three pairs of alternating layers, *i.e.*, $N = 6$. The innermost layer is taken as layer 1, whereas the outermost layer is taken as layer 2, with the layer sequence starting from the innermost layer, as 1/2/1/2/1/2, *i.e.*, the third and fifth layers have the same geometric and material properties as layer 1 and the fourth and sixth layers have the same geometric and material properties as layer 2. The non-dimensional material properties for layer 1 and layer 2 are taken as [13]

$$\begin{aligned} \bar{\rho}_{(1)} &= 1, & \bar{\mu}_{(1)} &= 0.254, & \bar{\lambda}_{(1)} &= 0.493, \\ \bar{\rho}_{(2)} &= 2.9, & \bar{\mu}_{(2)} &= 0.964, & \bar{\lambda}_{(2)} &= 0.972, \end{aligned} \quad (27)$$

In these non-dimensional quantities, the characteristic length, mass and time are taken as: the inner radius of the first layer R , the mass density of the first layer $\rho_{(1)}$ and $R/c_p^{(1)}$, where $c_p^{(1)}$ is the dilatational wave velocity in layer 1. In Eq. (27) and thereafter, the subscript or the superscript in between parenthesis denotes the quantity belonging to the k -th layer (where, in this example, $k = \overline{1, 6}$). The non-dimensional thickness of each layer is taken as $\bar{h}_{(1)} = \bar{h}_{(2)} = 1$ and the inner surface of the first layer is located at $\bar{R} = 1$. All properties given before correspond to those used by Turhan *et al.* [13], and the problem was treated in this reference as a one-dimensional wave propagation problem where the inner surface is subjected to only uniform radial pressure (thermal effects are neglected) with intensity p_o and the time variation of this uniform pressure is a step function with an initial ramp, see Fig. 3a, this pressure is zero at $t = 0$ and linearly rises to a constant value during the rising time $t_0 = 0.2$. The outer surface is taken free of surface traction, Eq. (9). In our analysis, this problem is treated as a special case whereas the constants a and b appear in Eqs. (6) and (18) are taken as $a = 1$ and $b = 0$. These restrictions reduce the layers of the problem to an elastic, linear and homogeneous layers, since the mass density and the stiffness of each layer become constant throughout the radial direction and the characteristic lines are thus composed of straight lines with constant slopes. In Figs. 4 and 5, the variations of the normal stresses (τ_{rr}/p_o) and ($\tau_{\theta\theta}/p_o$) with non-dimensional time at the location $\bar{r} = 2.5$ are shown. These results are identical with those obtained in Ref. [13]; and, hence, they are shown as the same curves in Figs. 4 and 5. These results provide further confidence in

the numerical technique employed in this study to treat transient wave propagation in a spherical FGM layered media. However, we have not found a suitable one-dimensional solutions in a spherical FGM composite for comparison. The curves of Figs. 4, 5 clearly display the effects of reflections and refractions from the inner and outer boundaries through the large sudden changes in the stress levels, the effects of reflections and refractions from the interfaces through the small sudden changes in the stress levels. The curves further show the effects of geometric dispersion and show that the numerical technique applied is capable of predicting the sharp variations in the neighborhood of the wave fronts without showing any sign of instability or noise.

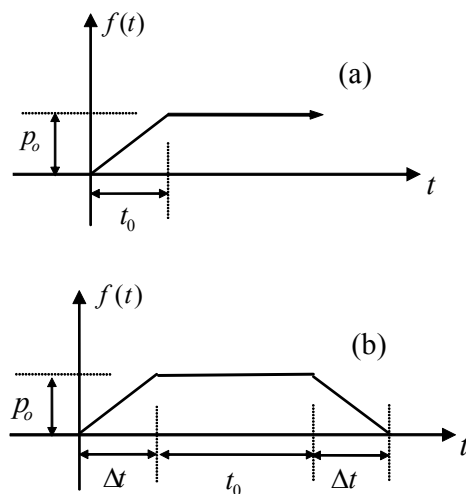


Figure 3: Time variations of the loads applied on the inner surface ($r = R$).

Now, we present some results for one-dimensional wave propagation in an FGM layer consists of nickel (*Ni*) and silicon (*SiC*). On one surface of the layer is pure nickel and on the other surface pure silicon, and the material properties in-between these two surfaces vary smoothly in the radial direction. The material properties of the constituent materials are given in Table 1. The numerical computations have been carried out and the results are displayed in terms of non-dimensional quantities. These dimensionless quantities are taken in terms of the inner radius R , the density and stiffness at the inner surface, *i.e.*, the following non-dimensional quantities will be always true on the surface of the inner boundary: $\bar{R} = (2\bar{\mu} + \bar{\lambda}) = \bar{\rho} = 1$. Note here that, the non-dimensional quantities are designated by bars. The

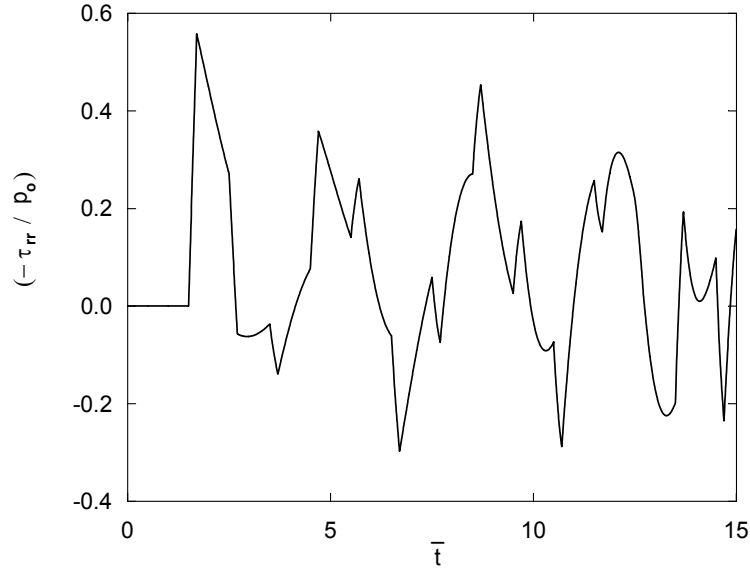


Figure 4: Variation of (τ_{rr} / p_o) with \bar{t} at $\bar{r} = 2.5$ for three pairs of alternating layers.

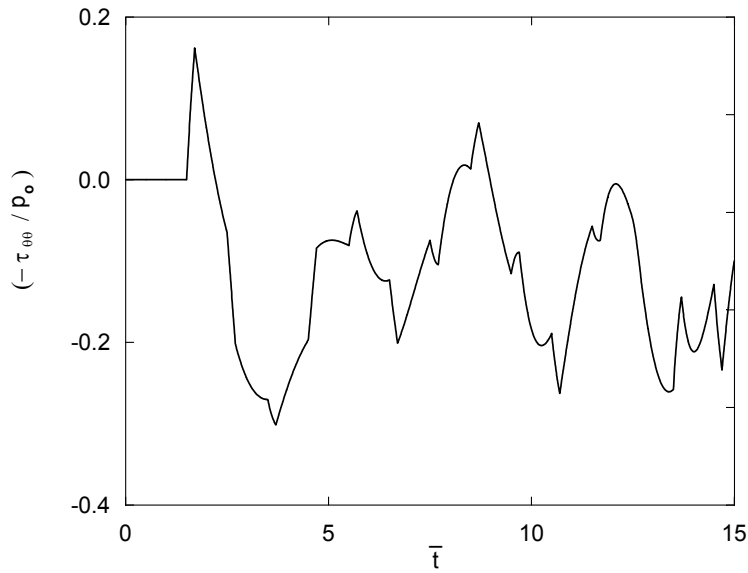


Figure 5: Variation of $(\tau_{\theta\theta} / p_o)$ with \bar{t} at $\bar{r} = 2.5$ for three pairs of alternating layers.

inner surface ($\bar{r} = \bar{R} = 1$) is subjected to a uniform normal stress defined by

$$\tau_{rr}(1, t) = -p_o(H(t) - H(t - t_o)), \quad (28)$$

where p_o is the intensity of load and $H(t)$ represents a unit step function with an initial ramp. Namely, the incident pressure wave applied on the inner surface is equivalent to the trapezoidal distribution shown in Fig. 3b, where \bar{t}_0 and $\bar{\Delta t}$ are taken as 0.25 and 0.001, respectively.

Table 1. Properties of materials used in examples.

	$\mu(GPa)$	$\lambda(GPa)$	$\rho(Kg/m^3)$
<i>Ni</i> (Nickel)	79	129	8900
<i>SiC</i> (Silicon)	90	46	3100

Here, we consider four different problems, all are subject to the trapezoidal pulse given by Eq. (28) and shown in Fig. 3b. These problems are: nickel-silicon (*Ni/SiC*) or silicon-nickel (*SiC/Ni*) FGM layer with free or fixed outer boundary conditions. The FGM spherical layer is assumed to be consisting of four similar layers with $\bar{h}_{(k)} = 0.25$ ($k = \overline{1, 4}$), where $\bar{h}_{(k)}$ is the non-dimensional thickness of the k -th layer, see Fig. 6. The thicknesses and the material properties of all the four layers are assumed to be the same. Thus, using the non-dimensionalization, the material properties defined by Eq. (6) for the four layers can be computed from Table 1 as:

for the *Ni/SiC* FGM layer with $m = n + 2$, see Fig. 6a,

$$\begin{aligned} m &= -0.58585, & n &= -2.58585, & a &= 0.4964, & b &= 0.5036, \\ \bar{\rho}_0 &= 1, & \bar{\mu}_0 &= 0.27526, & \bar{\lambda}_0 &= 0.44948, & \bar{c}_0 &= 1, \end{aligned} \quad (29)$$

and for the *SiC/Ni* FGM layer with $m = n + 2$, see Fig. 6b,

$$\begin{aligned} m &= -0.58588, & n &= -2.58588, & a &= 1.33492, & b &= -0.33492, \\ \bar{\rho}_0 &= 1, & \bar{\mu}_0 &= 0.39823, & \bar{\lambda}_0 &= 0.20354, & \bar{c}_0 &= 1. \end{aligned} \quad (30)$$

For various combinations of boundary conditions and material compositions shown in Fig. 6, the variation of normalized normal stresses τ_{rr}/p_o and $\tau_{\theta\theta}/p_o$ with the non-dimensional time \bar{t} at $\bar{r} = 1.25$ is given in Figs. 7–12. The curves in Figs. 7–10, correspond to free outer boundary conditions, while the curves of Figs. 11, 12 correspond to fixed outer boundary conditions. The dashed curves in these figures, Figs. 7–12, correspond to FGM layers with material properties given in Eq. (29) or (30), whereas the solid curves correspond to linear, homogeneous and

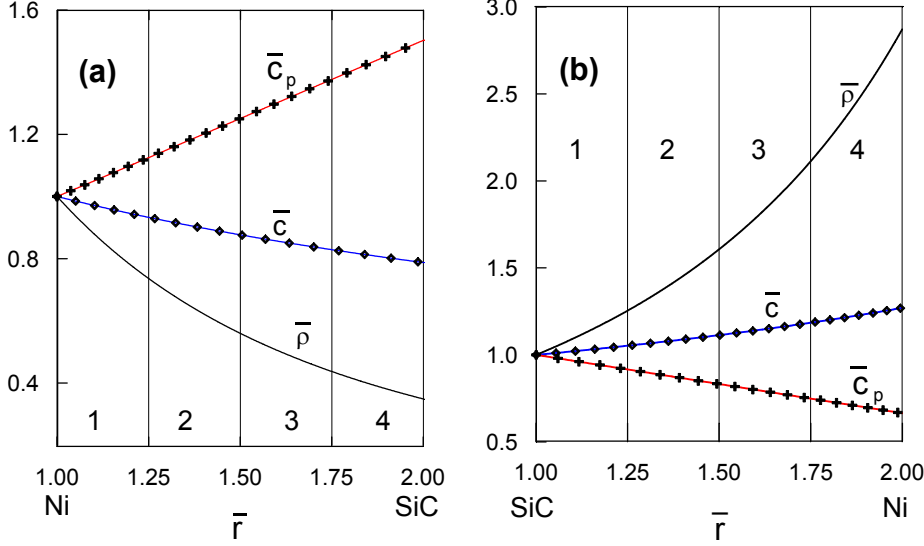


Figure 6: Variation of non-dimensional density ($\bar{\rho} = \frac{\rho}{\rho_0}$), stiffness ($\bar{c} = \frac{2\mu+\lambda}{2\mu_0+\lambda_0}$) and wave velocity (\bar{c}_p) with \bar{r} in (a) Ni/SiC FGM composite and (b) SiC/Ni FGM composite.

isotropic material. Since the properties of all the four layers are taken equal, the dashed curves in Figs. 7–12 represent \bar{R}_o solutions for a single FGM spherical layer with dimensionless outer boundary $\bar{R}_o = 2$ and with material properties given in Eq. (29) or Eq. (30). The curves corresponding to the homogeneous layer are obtained as a special case by assigning $a = 1$ and $b = 0$ in Eqs. (29–30); whereas, the propagation time of the dilatational wave (\bar{c}_p) through the non-dimensional thickness ($\bar{R}_o - \bar{R} = 1$) of the homogeneous layer is taken as $\bar{t} = 1$. The curves of Figs. 7–12 clearly show the effects of reflections at the inner and outer surfaces through the sudden changes in the stress levels. We note further that reflections and refractions from the interfaces have disappeared, this is due to the fact that the material properties vary smoothly in the radial direction. Moreover, we note that the stress levels in the homogeneous layer are higher than those correspond to the Ni/SiC FGM layer, Figs. 7, 8 and 11, and they are less than those correspond to the SiC/Ni FGM layer, Figs. 9, 10 and 12. These deviations from the homogeneous material are due to the fact that the inner boundary $\bar{r} = 1$ is the stiffer side in the Ni/SiC FGM layer, Fig. 6a, and if $\bar{r} = 1$ is the less stiff side, then the stress levels will be higher than the corresponding homogeneous layer. Because the wave velocity of the homogeneous layer ($\bar{c}_p = 1$) is less than that of the Ni/SiC FGM layer, Fig. 6a, the stress wave propagates faster in the Ni/SiC FGM layer, Figs. 7, 8 and 11.

However, the stress wave in the homogeneous layer is travelling faster than that in the *SiC/Ni* FGM layer, see Figs. 9, 10 and 12, this is clearly pronounced as time increasing. We, further, note that if the outer boundary is free of surface traction then the compressive waves are reflected as tensile waves from that boundary, Figs. 7–10, and they are reflected as compressive waves if the outer boundary is fixed, Figs. 11, 12.

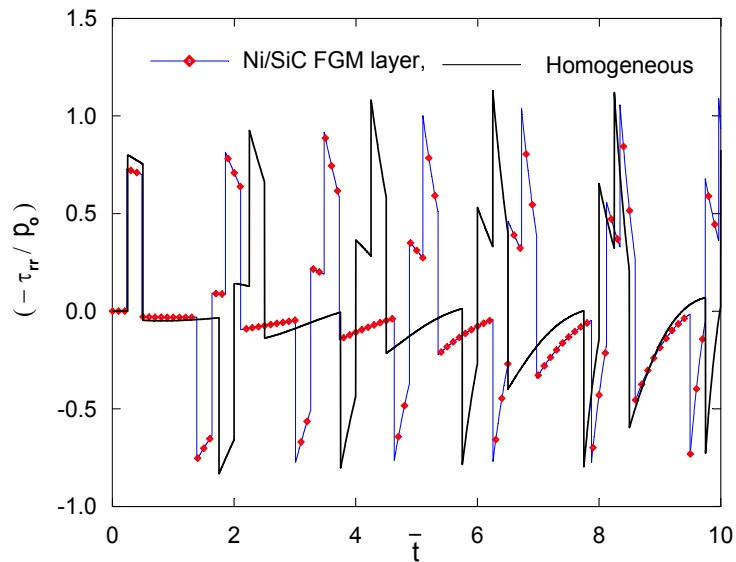


Figure 7: Variation of (τ_{rr} / p_o) with \bar{t} in *Ni/SiC* FGM layer and in homogeneous layer at $\bar{r} = 1.25$ under free/free boundary conditions.

5 Conclusion

The propagation of one-dimensional transient pressure waves in multilayered spherical FGM media consisting of N different layers is investigated. The material properties are assumed to be varying smoothly in the radial direction. By suitable adjusting the material properties, curves for homogeneous, linear and elastic multilayered spherical media are also obtained. The method of characteristics is employed to obtain the solutions of the considered initial-boundary value problem. The results show that the applied numerical technique is capable of predicting the sharp variations at the wave fronts without showing any sign of instability or noise. Furthermore, this technique is properly account for the effects caused by reflections and refractions of waves at the boundaries and interfaces between the layers and

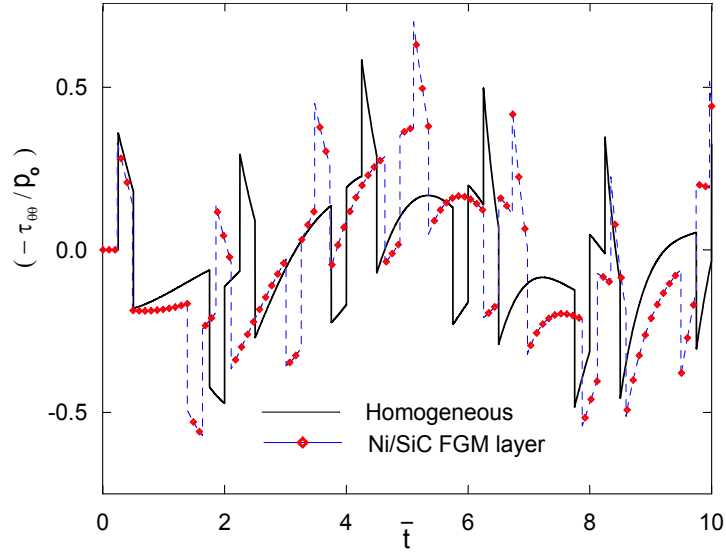


Figure 8: Variation of $(\tau_{\theta\theta} / p_o)$ with \bar{t} in *Ni/SiC* FGM layer and in homogeneous layer at $\bar{r} = 1.25$ under free/free boundary conditions.

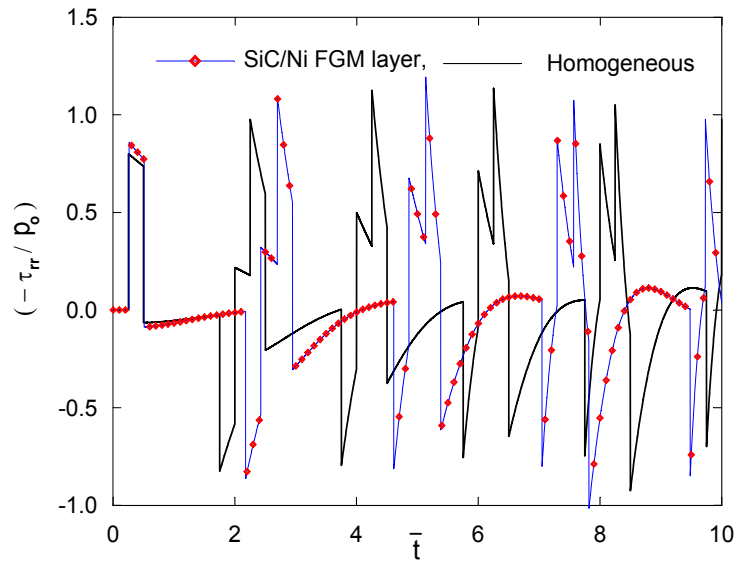


Figure 9: Variation of (τ_{rr} / p_o) with \bar{t} in *SiC/Ni* FGM layer and in homogeneous layer at $\bar{r} = 1.25$ under free/free boundary conditions.

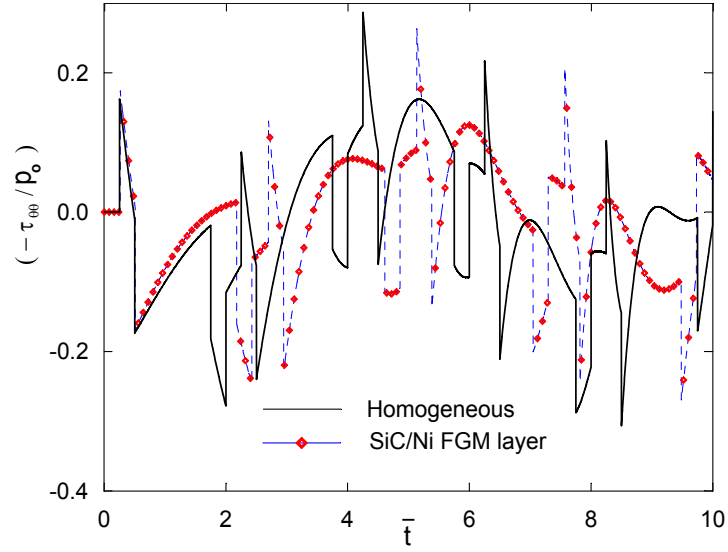


Figure 10: Variation of $(\tau_{\theta\theta} / p_o)$ with \bar{t} in *SiC/Ni* FGM layer and in homogeneous layer at $\bar{r} = 1.25$ under free/free boundary conditions.

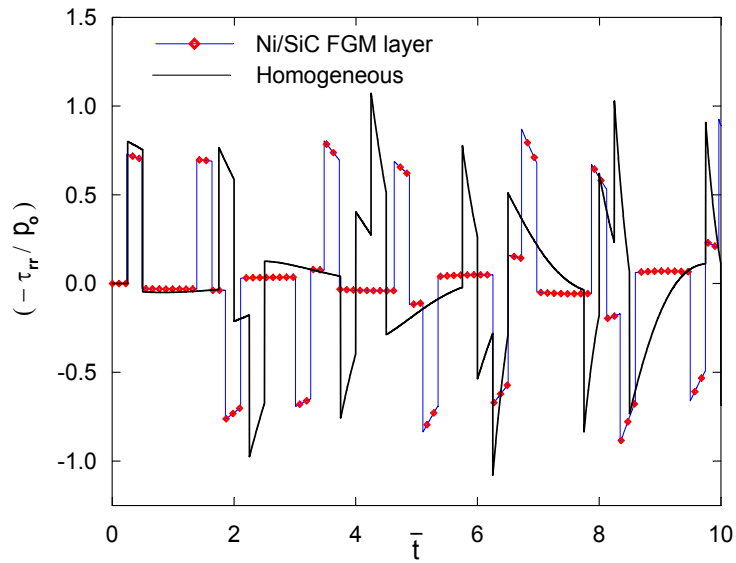


Figure 11: Variation of (τ_{rr} / p_o) with \bar{t} in *Ni/SiC* FGM layer and in homogeneous layer at $\bar{r} = 1.25$ under free/fixed boundary conditions.

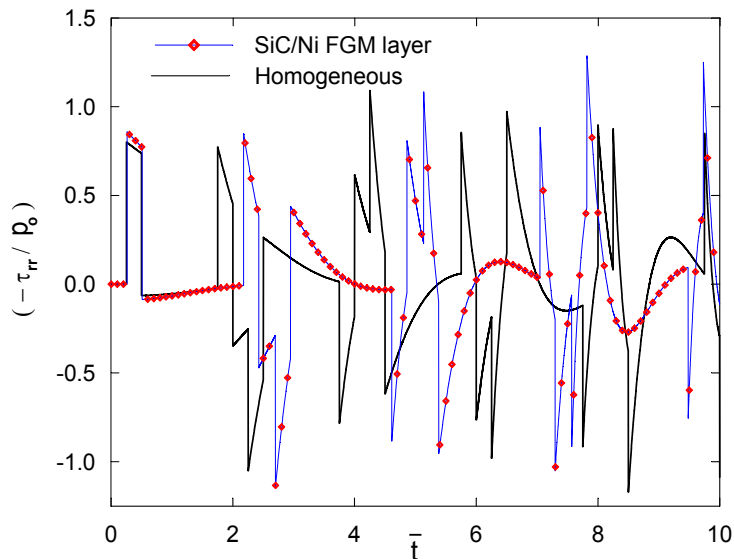


Figure 12: Variation of (τ_{rr} / p_o) with \bar{t} in *SiC/Ni* FGM layer and in homogeneous layer at $\bar{r} = 1.25$ under free/fixed boundary conditions.

the homogeneity effects in the wave profiles.

Based on the results obtained for an FGM layer one may conclude that: depending on the material property grading, location of the receiver point, boundary conditions and the amplitude of the input pulse, the resultant stress amplitudes may be greater or less than those applied at the inner boundary. It is pronounced that these amplitudes become less than those applied at the inner surface, when the inner surface ($r = R$) is stiffer than the outer surface ($r = R_o$) and become greater when the outer surface of an FGM layer is stiffer than the inner surface.

The method applied in this study can be combined with Fourier transform or Laplace transform and used effectively in investigating two-dimensional transient dynamic response in multilayered FGM media. The combined methods can further be applied effectively in other problems of practical importance, such as to the impedance analysis, either in frequency or time space. The determination of these impedance relations is important in performing soil-structure interaction analysis by substructure method. Our research in these directions is under way.

Acknowledgement

The authors would like to thank Dr. Ali Şahin, for his valuable suggestions and Mr. Ibrahim Karatay who assisted in preparing the manuscript.

References

- [1] YAMANOUCHI M., KOIZUMI M., HIRAI T. AND SHIOTA I., Proceedings of the First International Symposium on Functionally Graded Materials, 1990.
- [2] KOIZUMU M. *The concept of FGM*, Ceram. Trans. Funct. Grad. Mater., **34** (1993), 3–10.
- [3] BANKS-SILLS L., ELIASI R. AND BERLIN Y., *Modeling of functionally graded materials in dynamic analyses*, Composites Part B: Engineering, **33** (2002), 7–15, 2002.
- [4] LIU G. R. AND TANI J., *Surface waves in functionally gradient piezoelectric plates*, Journal of Vibration and Acoustics, **116** (1994), 440–448.
- [5] OHYOSHI T., *Linearly inhomogeneous layer elements for reflectance evaluation of inhomogeneous layers*, Dynamic Response and Behavior of Composites, **46** (1995), 121–126.
- [6] OHYOSHI T., *New stacking layer elements for analyses of reflection and transmission of elastic waves to inhomogeneous layers*, Mechanics Research Communication, **20** (1993), 353–359.
- [7] HAN X. AND LIU G. R., *Effects of waves in functionally graded plate*, Mechanics Research Communication, **29** (2002), 327–338.
- [8] LIU G. R., HAN X. AND LAM K. Y., *Stress Waves in functionally gradient materials and its use for material characterization*, Composites Part B: Engineering, **30** (1999), 383–394.
- [9] HAN X., LIU G. R. AND LAM K. Y., *A quadratic layer element for analyzing stress waves in functionally gradient materials and its application in material characterization*, Journal of Sound and Vibration, **236** (2000), 307–321.
- [10] CHIU T. C. AND ERDOĞAN F., *One-dimensional wave propagation in a functionally graded elastic medium*, Journal of Sound and Vibration, **222** (1999), 453–487.
- [11] BEREZOVSKI A., ENGELBRECHT J. AND MAUGIN G. A., *Numerical simulation of two dimensional wave propagation in functionally graded materials*, European Journal of Mechanics, **22** (2003), 257–265.
- [12] SANTARE M. H., THAMBURAJ P. AND GAZOANS G. A., *The use of graded finite elements in the study of elastic wave propagation in continuously non-homogeneous materials*, International Journal of Solids and Structures, **40** (2003), 5621–5634.

- [13] TURHAN D., CELEP Z. AND ZAIN-EDDIN I. K., *Transient wave propagation in layered media* Journal of Sound and Vibration, **144** (1991), 247–261.
- [14] MENGI Y. AND TANRIKULU A. K., *A numerical technique for two-dimensional transient wave propagation analyses*, Communication of Applied Numerical Methods, **6** (1990), 623–632.
- [15] WEGNER J. L., *Propagation of waves from a spherical cavity in an unbounded linear viscoelastic solid*, International Journal of Engineering Sciences, **31** (1993), 493–508.
- [16] ABU-ALSHAIKH I., TURHAN D. AND MENGI Y., *Two-dimensional transient wave propagation in viscoelastic layered media*, Journal of Sound and Vibration, **244** (2001), 837–858.
- [17] ABU-ALSHAIKH I., TURHAN D. AND MENGI Y., *Transient waves in viscoelastic cylindrical layered media*, European Journal Mechanics A/Solids **21** (2002), 811–830.
- [18] COURANT R. AND HILBERT D., *Methods of Mathematical Physics Vol. II.*, Interscience Publishers, New York, 1966.
- [19] WHITHAM G. B., *Linear and Nonlinear Waves*, Wiley, New York, 1974.
- [20] GERALD C. F. AND WHEATELY P. O., *Applied Numerical Analysis*, USA, 1984.